Journal of the European Ceramic Society **13** (1994) 467–484

The Oxidation Kinetics of β-Sialon Ceramics

Jeanette Persson & Mats Nygren

Department of Inorganic Chemistry, Arrhenius Laboratory, Stockholm University, S-106 91 Stockholm, Sweden

(Received 24 May 1993; revised version received 18 October 1993; accepted 23 November 1993)

Abstract

The oxidation behaviour of β-sialons ($Si_{6-z}Al_zO_zN_{8-z}$) with the composition z = 0·5 and 3·8, prepared without and with an addition of 3 and 6 wt% yttria, has been investigated isothermally during 20 h in a TG unit at temperatures between 1200 and 1450 C. A comparison is also given of the oxidation behaviour of β-sialons prepared from two Si_3N_4 powders with different amounts of impurities; and finally the oxidation behaviour of single-phase β-sialons with z = 1, 2·5 and 3·8 is compared with that of Si_3N_4.

Only a few of the obtained oxidation curves followed the parabolic rate law during the entire experiment. Most of the curves could, however, be interpreted with the modified rate law,

$$(\Delta w/A_0) = a\,arctan\,(bt)^{1/2} + c(t)^{1/2} + d$$

either exhaustively or in combination with the parabolic rate law. The parabolic rate constants and activation energies for the oxidation process could be determined and were found to increase with increasing amount of intergranular phase and with increasing amounts of impurities. The parabolic rate constants were also found to be lower for the β-sialons prepared without yttria than for 'pure' Si_3N_4, but the activation energy was about the same. The oxidation kinetics of the materials with z = 0·5 and 3 wt% yttria could not be conclusively determined, but the evolution of the microstructure of the oxide scale showed that its crystallization had an important influence on the oxidation rate.

Das Oxydationsverhalten von β-Sialonen ($Si_{6-z}Al_zO_zN_{8-z}$) mit den Zusammenzetzungen z = 0·5 und 3·8, hergestellt mit und ohne Zugabe von 3 bzw. 6 Gew.% Yttriumoxyd, wurde isotherm während 20 h in einer TG-Einheit bei Temperaturen zwischen 1200 und 1450 C untersucht. Weiterhin wird das Oxydationsverhalten von β-Sialonen, hergestellt aus zwei Si_3N_4-Pulvern mit verschiedenen Verunreinigungsgraden, verglichen. Schließlich erfolgt ein Vergleich des Oxydationsverhaltens einphasiger β-Sialone (z = 1, 2·5 und 3·8) mit dem Oxydationsverhalten von Si_3N_4.

Nur wenige der erhaltenen Oxydationskurven folgen während des gesamten Experiments einem parabolischen Ratengesetz. Die meisten Kurven konnten jedoch mit Hilfe eines modifizierten Ratengesetzes,

$$(\Delta w/A_0 = a\,arctan\,(bt)^{1/2} + c(t)^{1/2} + d$$

alleine oder in Verbindung mit dem parabolischen Ratengesetz beschrieben werden. Die parabolischen Ratenkonstanten und Aktivierungsenergien des Oxydationsprozesses konnten bestimmt werden; es zeigte sich, daß sie mit der Zunahme der Zwischenkornphase und mit höherem Verunreinigungsgrad zunehmen. Weiterhin ergab sich, daß die parabolischen Ratenkonstanten für β-Sialone, hergestellt ohne Yttriumoxyd, kleiner sind als die für 'reines' Si_3N_4, während die Aktivierungsenergien etwa gleich sind. Die Oxydationskinetik des Materials mit z = 0·5 und 3 Gew.% Yttriumoxyd konnte nicht eindeutig bestimmt werden, aber die Entwicklung des Gefüges der Oxydschicht zeigte, daß ihre Kristallisation einen entscheidenden Einfluß auf die Oxydationsrate hat.

Le comportement à l'oxydation de sialon β ($Si_{6-z}Al_zO_zN_{8-z}$) de composition z = 0·5 et 3·8, synthétisés avec addition de 3 et 6% en poids de Y_2O_3, a été étudiée par thermogravimétrie. Les mesures ont été réalisées dans des conditions isothermes pendant 20 h, à des températures comprises entre 1200 et 1450 C. Une comparison est également présentée entre les comportements à l'oxydation de deux sialons synthétisés à partir de deux poudres de Si_3N_4 contenant différentes quantités d'impuretés. Enfin, une comparison est également réalisée entre les comportements à l'oxydation de sialons β avec z = 1, 2·5, 3·8 et du Si_3N_4.

Journal of the European Ceramic Society 0955-2219/94/$7.00

Seules quelques unes des courbes d'oxydation obtenues suivent la loi de vitesse parabolique durant l'entièreté de l'expérience. La plupart des courbes pourraient cependant être interprétées avec la loi modifiée

$$(\Delta w/A_0) = a\,arctan\,(bt)^{1/2} + c(t)^{1/2} + d$$

soit de façon exhaustive, soit en combinaison avec la loi parabolique. Les constantes de vitesse de la loi parabolique et l'énergie d'activation du processus d'oxydation ont pu être déterminés et augmentent avec une augmentation de la quantité de phase intergranulaire et de la quantité d'impuretés. Les constantes de vitesse de la loi parabolique sont également plus faibles pour les sialons β préparés sans oxyde d'yttrium que pour un Si_3N_4 'pur', mais l'énergie d'activation est à peu près la même. La cinétique d'oxydation de matériaux avec z = 0·5 et 3% d'oxyde d'yttrium n'a pas pu être déterminée de façon concluante, mais l'évolution de la microstructure de la partie oxydée montre que sa cristallisation a une influence importante sur la vitesse d'oxydation.

1 Introduction

A pure Si_3N_4 ceramic is found to be extremely oxidation resistant, as a protective layer of SiO_2 is formed on its surface upon oxidation. The growth of this layer is in most cases reported to follow a parabolic rate law,

$$(\Delta w/A_0)^2 = K_p t + b \qquad (1)$$

where $\Delta w/A_0$ is the weight gain per unit area, K_p, the parabolic rate constant, t, the time, and b is an additive constant; and the oxidation rate is controlled by the diffusion of oxygen through the oxide scale.[1-5] The oxidation rate of Si_3N_4 is found to be even slower than the oxidation rate of Si, SiC and $MoSi_2$, which all form the same type of protective layer. This difference has been ascribed to the presence of an Si_2N_2O layer between the silica and the silicon nitride, implying that the oxygen diffusion through this layer is the rate-determining step.[3,6] The formation of Si_2N_2O has also been predicted by thermodynamic calculations.[7]

Other oxidation experiments with Si_3N_4 have, however, shown that the parabolic rate law, if ever, is obeyed only after an initial time lapse, t_0.[8,9] This deviant behaviour has been ascribed to a progressive crystallization of the amorphous phase in the oxide scale. As oxygen diffuses more easily in an amorphous phase than in a crystalline, partial crystallization of the amorphous phase causes a progressive decrease of the cross-section area through which the oxygen mainly diffuses. A new rate law, which takes this decrease of the area into account, has recently been developed, and reads:[8]

$$(\Delta w/A_0) = a\,\arctan\,(bt)^{1/2} + c(t)^{1/2} + d$$

This rate law will be reviewed later.

Because the self diffusion in Si_3N_4 is extremely slow, a sintering aid is usually added in order to produce dense materials through liquid-phase sintering.[10] Glass-forming oxides such as Y_2O_3, Al_2O_3, MgO and lanthanide oxides are customarily used as sintering aids. The use of sintering aid, however, leads to formation of a polyphasic material, i.e. the liquid forms residual intergranular phase(s) after sintering. If an Al_2O_3/AlN combination is used, then aluminium and oxygen can replace silicon and nitrogen in Si_3N_4, and a solid solution called β-sialon is formed, with the general composition $Si_{6-z}Al_zO_zN_{8-z}$ ($z \leq 4$). This substitution makes it possible to synthesize materials with a minimum content of intergranular phase.

The oxidation behaviour of these polyphasic materials is more complex than that of pure Si_3N_4. Si_3N_4 ceramics prepared with MgO or Y_2O_3 have been extensively studied and have been found to exhibit an oxidation resistance that is dependent both on the nature and the amount of the additional phases. During the oxidation process the cations in the intergranular phase diffuse into the oxide scale, and a depleted zone is formed underneath the scale. The intergranular glassy phase thus acts as a pathway for rapid diffusion within the material.[11-14] It has been shown that the oxidation rate is independent of the partial pressures of oxygen and nitrogen, implying that oxygen diffusion through the oxide scale is not rate determining.[14,15]

It has further been found, for Si_3N_4 sintered with MgO, that continued oxidation after removal of the oxide scale proceeds almost at the same rate as just before the removal, also implying that the oxide scale is only marginally protective.[15,16] The oxidation process has been interpreted with use of the parabolic rate law, and the diffusion of the intergranular cations into the oxide scale is believed to be the rate-limiting process, and that the reaction of the metal oxides with SiO_2 to form silicates is the driving force. The diffusion of the additive cations into the oxide scale results in an internal oxidation of Si_3N_4 to form Si_2N_2O in the depleted zone and the N^{3-} released will diffuse to the oxide scale as charge balance to the intergranular cations.[1,11,12]

It has, however, for Si_3N_4 sintered with Y_2O_3, also been reported that the removal of the oxide scale to some extent increased the oxidation rate, indicating that the oxide is somewhat protective, and that the oxidation rate could not entirely be determined by the diffusion rate of the intergranular cations into the oxide scale.[17-20] The importance of

the diffusion of oxygen and intergranular cations on the oxidation rate has, however, so far not been entirely clarified.

Even though most oxidation processes have been interpreted with the parabolic rate law, there have been reports claiming that the oxidation does not follow the rate law[18,21–23] or that it is applicable only after a certain time lapse.[24,25] Furthermore, it has been reported that the exponent, n, in the rate law $(\Delta w/A_0)^n = kt$ changes from 1 to 6 during the oxidation.[26,27] The oxidation of $Si_{6-z}Al_zO_zN_{8-z}$ sialon ceramics, prepared with and without additions of yttria, has been investigated and deviations from the parabolic rate law have been found. The applicability of the arctan rate law to the present results will be demonstrated.

This paper comprises two parts. In the first part the oxidation behaviour of β-sialons with $z = 0{\cdot}5$ and 3·8 prepared without and with 3 and 6 wt% Y_2O_3 is compared, as well as the oxidation behaviour of three of the compositions prepared from two Si_3N_4 powders with different amounts of impurities. In the second part, the oxidation behaviour of Si_3N_4 (previously published in Ref. 8) is compared with those of single-phase β-sialons with $z = 1$, 2·5 and 3·8.

As already mentioned, the arctan rate law has been developed assuming that the cross-section area for oxygen diffusion decreases with time. Thus, a function $A(t)$, which describes the time dependence of this decrease, is incorporated into the parabolic rate law in the following way

$$\frac{\mathrm{d}}{\mathrm{d}t}\left(\frac{\Delta w}{A_0}\right) = \frac{\sqrt{K_p}A(t)}{2\sqrt{t}} \tag{2}$$

To be able to explain the experimental observations, the selected $A(t)$ function must, besides containing a rate constant, have the following properties:

(i) $A(t)$ should be able to attain the value one over the entire experimental time, i.e. if no devitrification of the oxide scale occurs, integration of eqn (2) should yield the parabolic rate law.

(ii) $A(t)$ should be able to decrease to a value between one and zero at the end of the experiment, which experimentally would correspond to a decrease of the cross section area available for the diffusing species during the entire experimental time, i.e. a nonparabolic rate law behaviour is observed during the entire experimental time.

(iii) in order to be able to describe the oxidation curves, which are nonparabolic in the beginning of the experiment but exhibit a parabolic oxidation behaviour at the end, the $A(t)$ function has to contain a constant t_0, which defines the time at which the oxidation process transforms from a nonparabolic to a parabolic one.

Considering these constrains an $A(t)$ function has been deduced which reads

$$A(t) = \frac{(1 + (f\beta - t_0^{-1})t)}{(1 + (\beta - t_0^{-1})t)} \tag{3}$$

where β is the rate constant for the decrease of the area, t_0 is the time at which the oxidation process transforms from a non-parabolic to a parabolic behaviour, i.e. a steady state is reached, and for $t > t_0$ the decrease of the area is negligible. f is the fraction of the unit area remaining at $t = t_0$. A simple exponential function with the desired properties has not been found.

By incorporating eqn (3) in eqn (2) and integrating, the new rate law is obtained reading:

$$\frac{\Delta W}{A_0} = a \arctan\sqrt{bt} + c\sqrt{t} + d \tag{4}$$

where

$$a = \frac{\beta\sqrt{K_p}(1-f)}{b^{3/2}} \quad b = \beta - t_0^{-1} \quad c = \frac{\sqrt{K_p}(f\beta - t_0^{-1})}{b}$$

$$K_p = (a\sqrt{b} + c)^2 \quad f = \frac{\dfrac{a\sqrt{b}}{bt_0 + 1} + c}{a\sqrt{b} + c} \tag{5}$$

and d = an additive constant ideally equal to zero.

If t_0 is reached within the time of the experiment, a parabolic behaviour is observed for $t > t_0$, as $A(t) = f$. This parabolic function is expressed as

$$(\Delta w/A_0)^2 = K_p^0 t + B_0 \tag{6}$$

where K_p^0 is an apparent rate constant and B_0 an additive constant >0. As the derivatives of the arctan and the parabolic functions are equal at $t = t_0$, the relation between K_p and K_p^0 becomes

$$K_p = \frac{K_p^0 t_0}{f^2\left(t_0 + \dfrac{B_0}{K_p^0}\right)} \tag{7}$$

A more elaborate description of the rate law is found in Refs 8, 25 and 26.

2 Experimental

Single-phase β-sialon samples of the composition $Si_{6-z}Al_zO_zN_{8-z}$, with z-values of 0·5, 1, 2·5 and 3·8, were prepared by mixing α-Si_3N_4 powder (H. C. Starck, Berlin, Germany, grade LC-10 or UBE, Japan, grade SN-10E) with Al_2O_3 (Alcoa, grade A16SG) and AlN (H. C. Starck, grade A). β-Sialon ceramics with $z = 0{\cdot}5$ and 3·8 were also prepared,

Table 1. Characteristic data of the starting Si_3N_4 powders

Si_3N_4 powder	α-phase (%)	Specific surface area (m^2/g)	Impurities (wt%)				
			Fe	Al	Ca	O	C
UBE 10-E	>95	10	<0·01	<0·005	<0·005	1·3	<0·1
Starck LC-10	96	11	0·02	0·04	0·004	1·7	0·17

with additions of 3 and 6 wt% Y_2O_3 (H. C. Starck, 99·9%) as sintering aid. Some of these compositions (see Table 2 later) were prepared using Si_3N_4 powder from both UBE and Starck. The Starck powder has a higher concentration of impurities than the UBE powder. Characteristic data for the two different Si_3N_4 powders are given in Table 1. The powders were carefully weighed in, also taking into account the oxygen content of the Si_3N_4 and AlN materials. The green bodies were glass-encapsulated and hot isostatically pressed at 1750°C for 2 h with 200 MPa of argon, to obtain dense materials. The prepared ceramics are labelled as 0·5:3:S, where the first figure represents the z-value, the second the amount (wt%) of yttria added and the final letter denotes the source of the Si_3N_4-powder used (S for Starck and U for UBE).

The crystalline phases present in the ceramics were identified from their X-ray powder pattern obtained in a Guinier–Hägg Camera with Cu$K\alpha_1$ radiation. The composition, i.e. the z-value of the β-sialon phase, was calculated from the formula $a = 0{\cdot}7603 + 0{\cdot}00297z$ nm and $c = 0{\cdot}2907 + 0{\cdot}00255z$ nm.[28] The density of the compacts was determined using Archimedes' principle in toluene and water. The amounts of intergranular phase (vol.%) were determined from the different contrast of the phases in SEM micrographs, using the image processing system, Kontron IBAS/IPS, online with the SEM, JSM 880.

Pieces of an approximate $15 \times 5 \times 1\,mm^3$ size were used for the oxidation experiments. They were carefully polished with diamond grains down to a size $< 1\,\mu m$, and a small hole was drilled through each piece, serving to attach it to the hangdown wire in the TG unit. Before oxidation, the pieces were cleaned in toluene, and in acetone in an ultrasonic bath. They were then oxidized isothermally in flowing oxygen for 20 h, at room temperatures ranging from 1200 to 1450°C, in the TG unit SETARAM TAG 24. The TG unit has two symmetric furnaces, one used for the oxidation of the sample and the other for an inert reference material. By regulation of the gas flow through the two furnaces, the drift of the baseline can be kept within $\pm 5\,\mu g$ for the 20 h duration of the experiment. The low drift makes it possible to record very accurate weight gains associated with the oxidation.

Complementary oxidation experiments of shorter duration have also been performed in order to obtain information about the evolution of the microstructure of the oxide scales as a function of time. Pieces of the ceramic were put on a platinum net and inserted into a preheated furnace, with oxygen flowing through. The pieces were pulled out from the furnace after different times of oxidation and cooled to room temperature.

The crystalline phases formed in the oxide scale were identified from the diffraction patterns recorded with an X-ray powder diffractometer operated in reflection mode (STOE, STADI). The surfaces and the cross-sections of the oxide scales were characterized with a scanning electron microscope (JSM 880) and by means of energy-dispersive X-ray analysis (LINK AN 10000). All the micrographs shown in this paper have been obtained with back-scattered electrons.

3 Results and Discussions

3.1 A comparison of the oxidation behaviour of β-sialons with $z = 0{\cdot}5$ and 3·8 prepared with 0, 3 and 6 wt% Y_2O_3

3.1.1 Characterization of the prepared samples

SEM studies of polished cross-sections of the prepared materials showed that fully dense β-sialon ceramics had been obtained. Densities, cell parameters, crystalline phases present and amount and composition of the intergranular glass in the different materials are given in Table 2. The composition of the intergranular glass could, however, only be determined for the sialons with a z-value of 3·8, as the multigrain pockets in the $z = 0{\cdot}5$ ceramic were too small to allow EDS analysis. The microstructure of the sialons with $z = 0{\cdot}5$ differs from that at $z = 3{\cdot}8$ as shown in Fig. 1. The grain size is smaller for the lower z values. There is also a clear difference between the microstructures of the 0·5:3:S and 0·5:3:U materials, but the microstructures of the corresponding materials with $z = 3{\cdot}8$ are very similar.

3.1.2 Oxidation curves and characterization of oxide scales

The oxidation curves for the materials prepared from Starck powder are shown in Fig. 2(a) and Fig. 3(a)–(d). The weight gain curves obtained during

Table 2. Properties of the β-sialon materials

Designated z-value	*Wt-% Y_2O_3*	*Si_3N_4 powder*[a]	*a-axis nm*	*c-axis nm*	*calc. z value*	*Density g cm^{-3}*	*Vol.% glass*	*Si:Al:Y ratio in the intergr. glass*
0·5	0	S	0·761 7	0·201 9	0·47	3·160	—	—
0·5	3	S	0·760 2	0·292 0	0·54	3·206	4–5	—
0·5	6	S	0·762 2	0·291 9	0·55+	3·248	3·5–4·5	—
0·5	3	U	0·761 7	0·291 7	0·45	3·178	4–5	—
3·8	0	S	0·771 1	0·300 3	3·70	3·051	—	—
3·8	3	S	0·771 0	0·299 8	3·58*	3·106	5–6	1:1·1–1·4:0·7–0·9
3·8	6	S	0·770 5	0·299 3	3·40**	3·138	7–8	1:1·2–1·3:1·0–1·3
3·8	0	U	0·770 0	0·300 0	3·56	3·052	—	—
3·8	3	U	0·760 6	0·299 8	3·52#	3·084	5–6	1:1·0–1·5:0·8–1·1

[a] S = Starck, U = UBE
Additional phases: +, 4 v-% α-sialon; *, 5 vol-% 15R; **, 10 vol-% 15R; #, minor amounts of X-phase.

oxidation of the β-sialons with $z = 0·5$ and 3·8, prepared without addition of Y_2O_3, are shown in Fig. 2(a). It is clearly seen that the oxidation resistance, i.e. the $(\Delta w/A_0)$ value reached after 20 h oxidation, is much better for $z = 0·5$ than for $z = 3·8$. At 1450°C, however, both materials are oxidized considerably.

The oxide scales formed on 0·5:0 are coherent and consist of a silica glass and minor amounts of α-cristobalite. The scales formed on 3·8:0, however, contain a considerable amount of mullite crystals and nitrogen bubbles which makes the surface look rough.

The weight gain is plotted in Fig. 3 as a function of oxidation time for $z = 0·5$((a) and (c)) and $z = 3·8$ ((b) and (d)) prepared with 3 and 6 wt% Y_2O_3. The

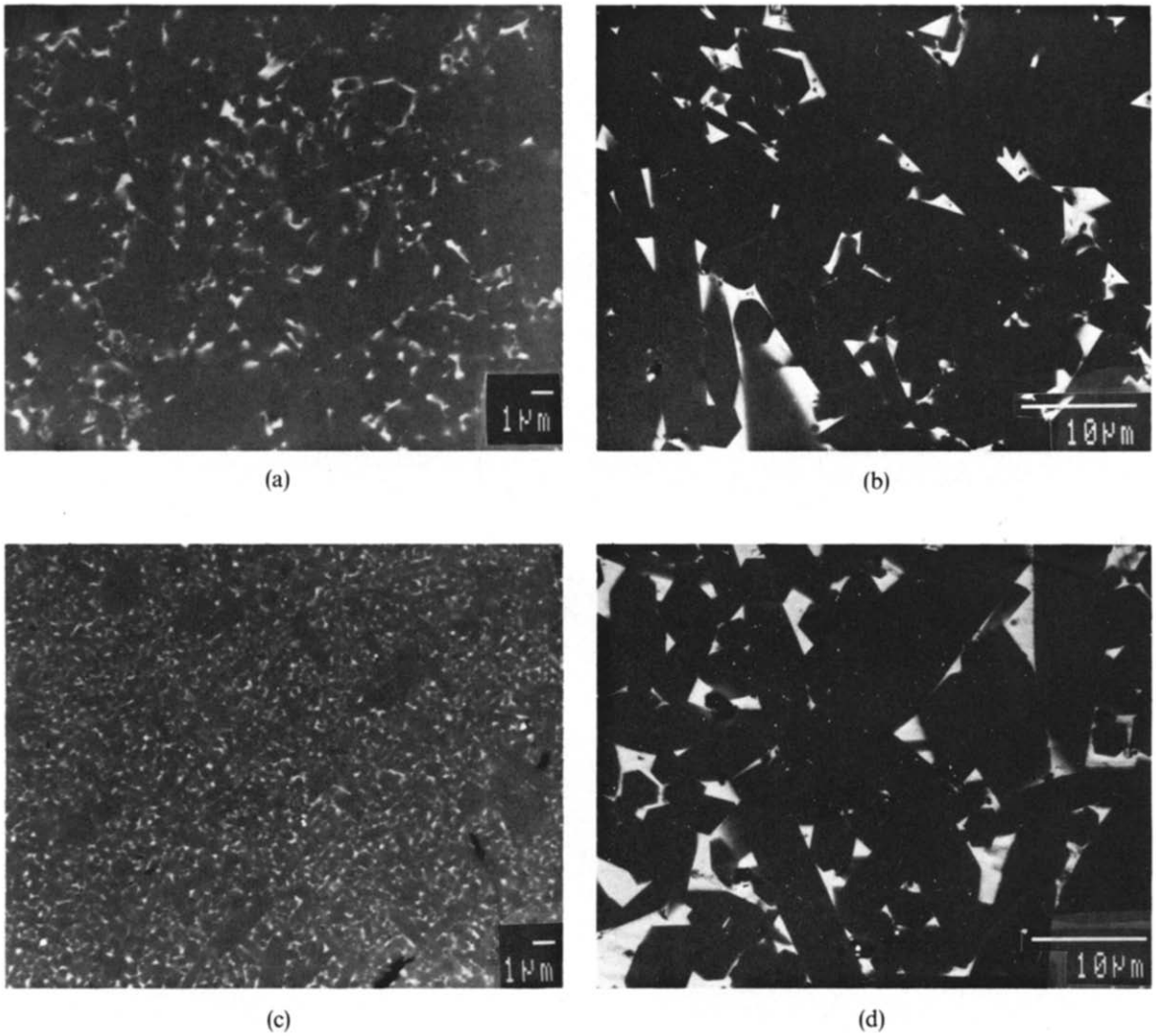

Fig. 1. The microstructure of the β-sialons (a) 0·5:3:S, (b) 3·8:3:S, (c) 0·5:3:U and (d) 3·8:3:U. The dark areas correspond to the β-sialon grains and the light areas to the intergranular glassy phase.

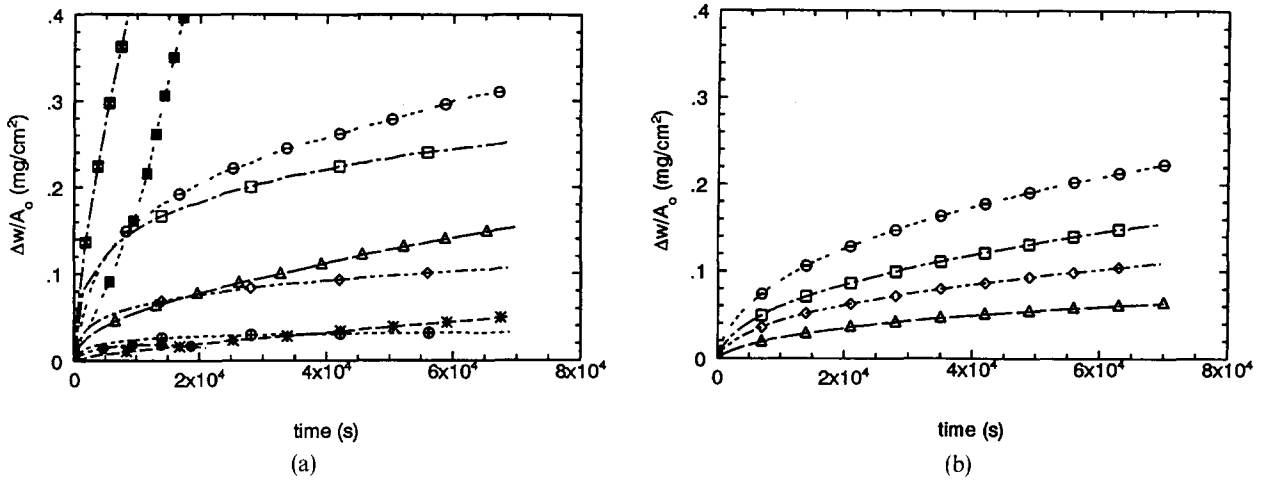

Fig. 2. The weight gain curves recorded in the oxidation of β-sialons with the compositions (a) 0·5:0:S and 3·8:0:S and (b) 3·8:0:U. △, 1250°C; ●,◇, 1300°C; ⊕,□, 1350°C; ∗,⊖, 1400°C; ■,⊠, 1450°C. ●,⊕,∗,■, 0·5; △,◇,□,⊖,⊠, 3·8.

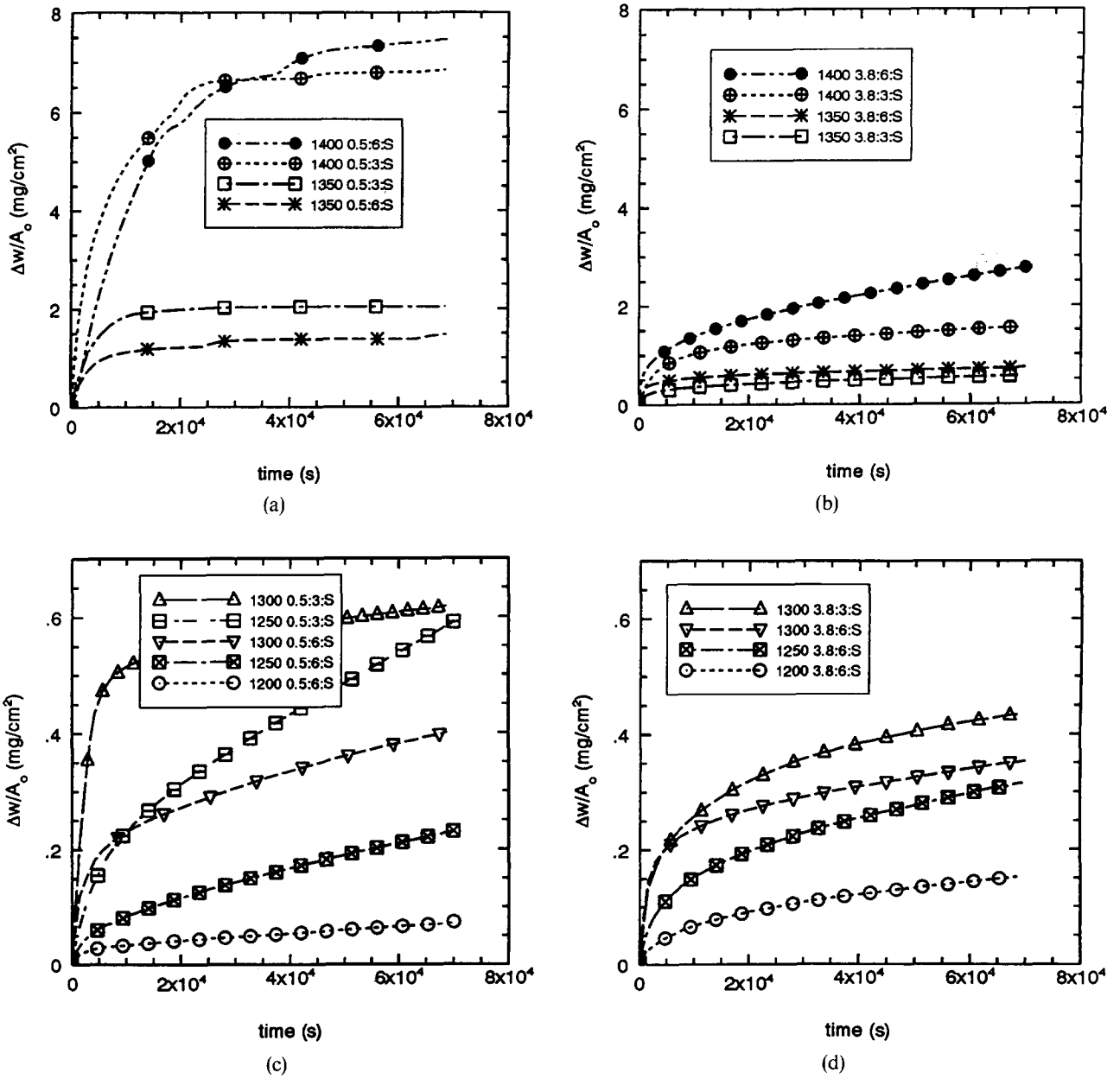

Fig. 3. The oxidation curves recorded for the materials 0·5:3:S ((a) and (c)) and 3·8:3:S ((b) and (d)) at $T \geq 1350$°C ((a) and (b)) and at $T < 1350$°C ((c) and (d)).

figures show that the oxidation resistance is better for ceramics with $z = 0{\cdot}5$ containing 6 wt% yttria than for those prepared with 3 wt%. The weight gain is somewhat irregular for 0·5:6 at 1350°C and for 0·5:6 and 0·5:3 at 1400°C, sudden increases of the weight gain are observed occasionally. This is most probably caused by nitrogen bubbles bursting through the protective oxide scale, cracking its surface and thereby reducing its mean thickness. This type of a sudden increase of the oxidation rate is not observed for the sialons with $z = 3{\cdot}8$. The final weight gain is higher for 3·8:6 than for 3·8:3 at $T > 1300$°C, in contrast to the findings of the corresponding materials with $z = 0{\cdot}5$. A lower final weight gain is, however, observed at 1300°C for the $z = 3{\cdot}8$ material with the highest content of yttria. (The material 3·8:3:S has not been oxidized at lower temperature.) In general it can be noted that the oxidation resistance is better during the 20-h oxidation experiments for $z = 0{\cdot}5$ than for $z = 3{\cdot}8$ at $T < 1300$°C but better for $z = 3{\cdot}8$ at $T \geq 1300$°C.

The oxide scales consist mainly of crystalline components, particularly at the surface. The phases present in the scale on the materials with $z = 0{\cdot}5$ are $Y_2Si_2O_7$, α-cristobalite, mullite (minor amounts) and a glass containing Y, Si and Al. At the lower temperatures (1250, 1300°C) the $Y_2Si_2O_7$ crystals almost completely cover the surface of the oxide scale; underneath this surface scale a glassy phase is found, and closest to the sialon matrix there is a layer of α-cristobalite. With increasing temperature the amount of $Y_2Si_2O_7$ decreases, while the amounts of α-cristobalite and glass and the concentration of Y and Al in the glass increase, see Fig. 4(a)–(c). At 1400°C the oxide scale is mainly composed of α-cristobalite and 'pockets' containing a glass. The Si:Al:Y ratio of the glass phase present in the oxide scale on the 0·5:3:S material is 1:0·2:0·1 at 1300°C, 1:0·3:0·2 at 1350°C and 1:0·4:0·3 at 1400°C.

The oxide scales formed on sialons with a z-value of 3·8 show a similar morphology as those obtained for $z = 0{\cdot}5$, but the relative amounts of the crystalline phases present are different, and in addition phases such as $Y_3Al_5O_{12}$ (YAG) and $YAlO_3$ are found. The oxide scales formed on $z = 3{\cdot}8$ seem to comprise less glass and more Y-containing crystals than

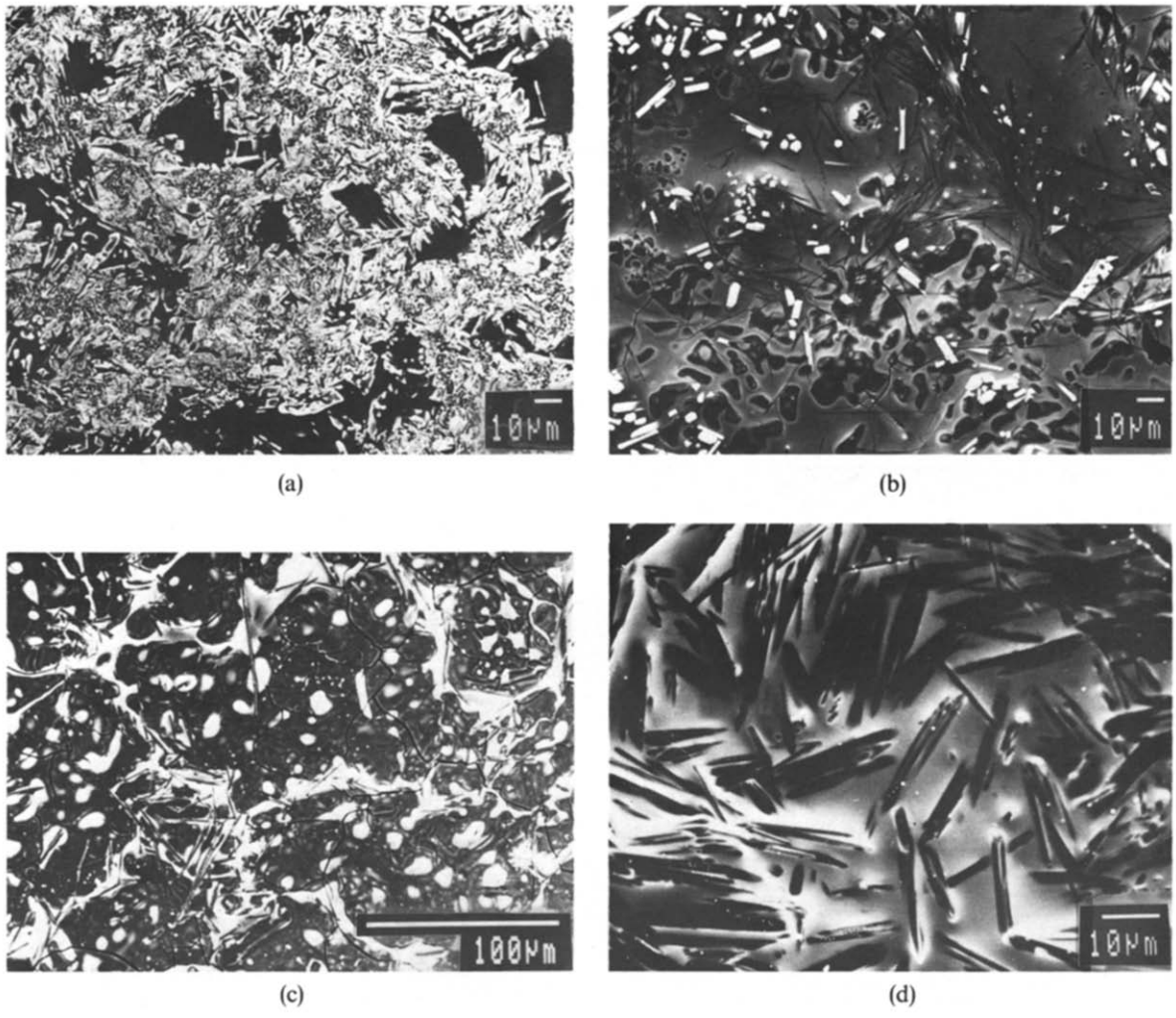

Fig. 4. The surface of the oxide scales formed on the β-sialon of the composition 0·5:3:S at (a) 1300°C, (b) 1350°C and (c) 1400°C and on the β-sialon 3·8:6:3 at (d) 1400°C. In (a) and (b) the surface consists of $Y_2Si_2O_7$ (the light crystals), mullite (the needle-like crystals), a glass and α-cristobalite (the darkest areas in (b)). The surface in (c) consists of α-cristobalite and mullite and the Y is present only in a glassy phase; and in (d) of mullite crystals in a glass (light area).

observed for $z = 0{\cdot}5$. The composition of the glassy phases in the oxide scales could not be determined for $T < 1400°C$. At 1400°C, however, the main phase in the scale is a Y–Si–Al–O glass, and the mullite crystals are found in the glass matrix (see Fig. 4(d)). The amount of mullite is highest close to the sialon material. The different microstructure of the oxide scales on the sialons with $z = 0{\cdot}5$ and 3·8 at $T \geq 1350°C$ could explain why the oxidation resistance is drastically decreased for the sialon with $z = 0{\cdot}5$. The relatively low amount of glass and high amount of α-cristobalite compared to the opposite relationship between glass and mullite for $z = 3{\cdot}8$, prevent the oxide layer from self-healing as nitrogen breaks through the oxide surface, but cracks in the oxide scale will remain. This is not the case for $z = 3{\cdot}8$, where the glass almost covers the surface, which is therefore self-healing.

The Si:Al:Y ratio in the glassy phases present in the oxide scale on the materials oxidized at 1400°C is 1:0·4:0·3 (0·5:3:S), 1:0·5:0·5 (0·5:6:S), 1:0·4:0·4

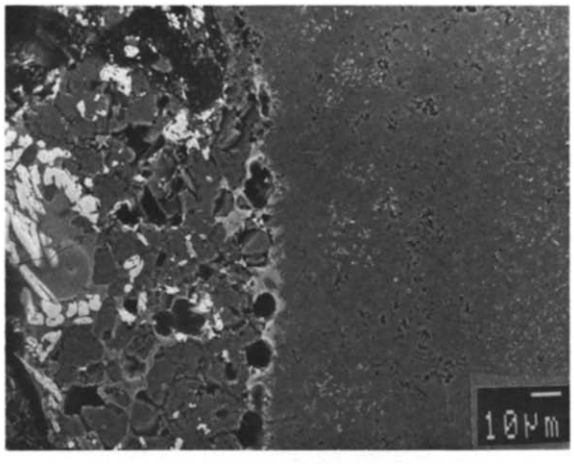

(a)

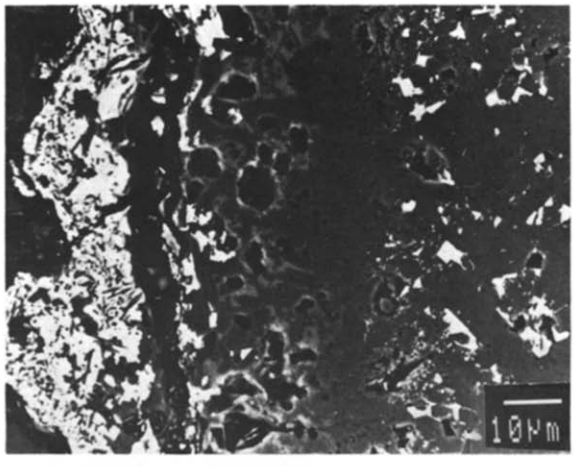

(b)

Fig. 5. Cross-sections of the oxide scale formed at 1350°C on the material (a) 0·5:6:S and (b) 3·8:6:S, illustrating the wider Y-depleted zone formed in 0·5:6:S. The oxide scales are recognized in the left part of the figures and the sialon matrix in the right part. The brightness indicates the Y-content of the different phases. A high Y-concentration gives a bright contrast.

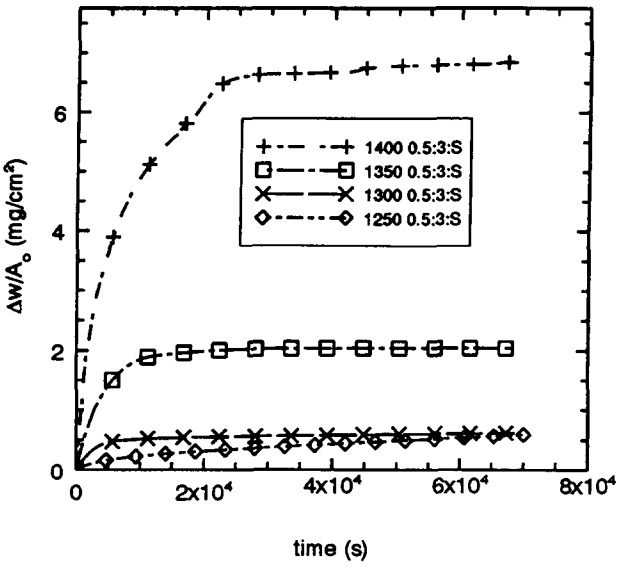

(a)

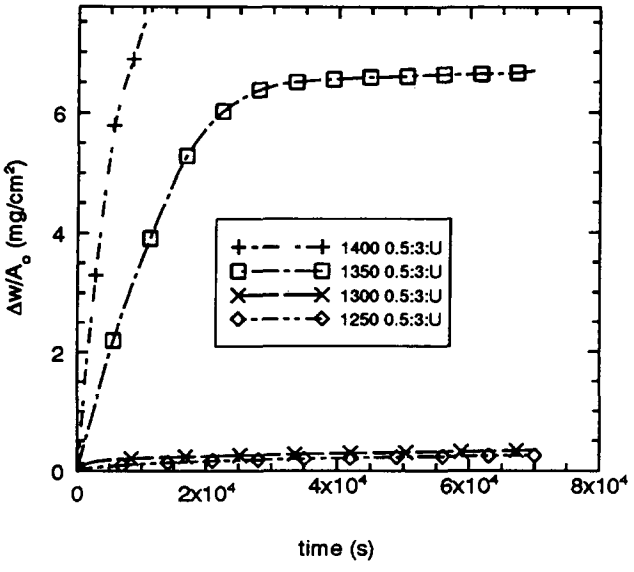

(b)

Fig. 6. A comparison of the oxidation behaviour of the β-sialons with the composition $z = 0{\cdot}5$ and 3 wt% yttria prepared with Si_3N_4 powder (a) from Starck and (b) from UBE.

(3·8:3:S) and 1:0·5:0·3 (3·8:6:S). Thus, only small differences are found for the ceramics at 1400°C. Below the oxide scale there is a zone depleted in yttrium. This depleted zone has been found to be more extended for $z = 0{\cdot}5$ than for 3·8, see Fig. 5(a) and (b). It is also observed that the sialon matrix with $z = 3{\cdot}8$ undergoes transformations during the oxidation process. A partial crystallization of the intergranular phase occurs, whereby YAG is formed, which will decrease the mobility of the intergranular ions. The intergranular phase in the materials with $z = 0{\cdot}5$ seems, however, to remain unchanged during the oxidation.

In Fig. 6(a) and (b), Fig. 7(a) and (b) and Fig. 2(a) and (b), the oxidation resistance of the sialon ceramics prepared from the Si_3N_4 Starck powder (a) is compared with the oxidation resistance of the UBE powder ceramic (b) for the compositions 0·5:3,

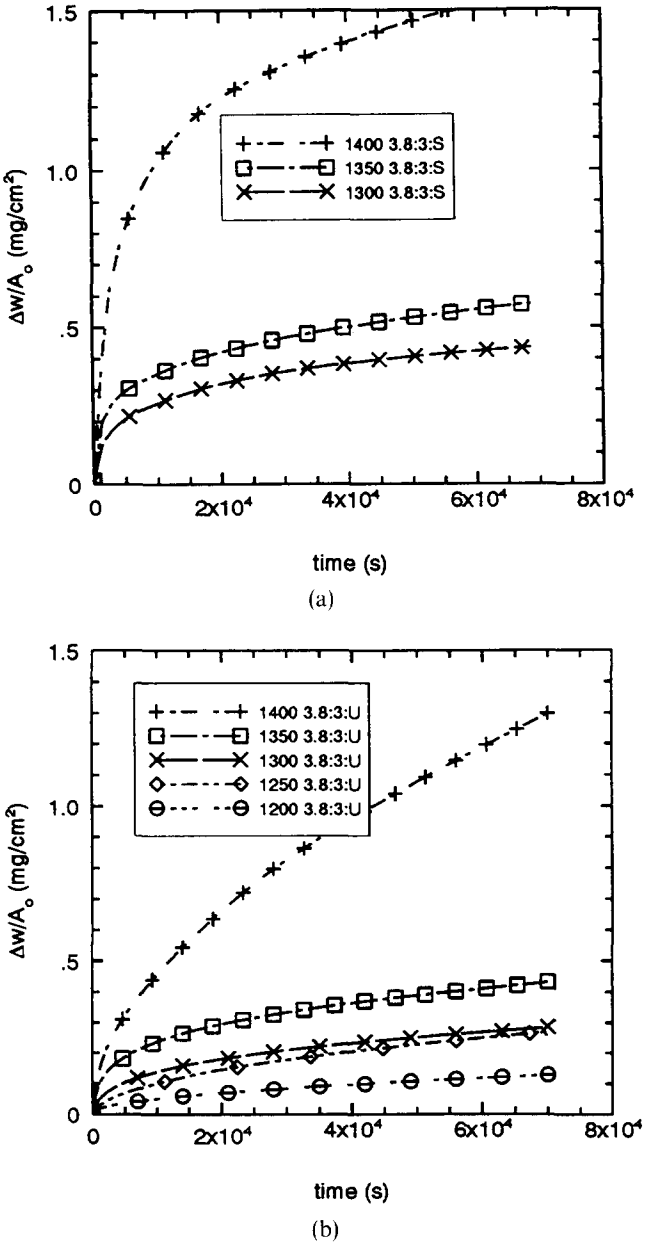

Fig. 7. The weight gain as a function of time for (a) 3·8:3:S and (b) 3·8:3:U.

3·8:3 and 3·8:0. The weight gain curves show that there is a clear difference in the oxidation behaviour of the samples prepared from the different powders. The oxidation resistance of 0·5:3:U is better than that of 0·5:3:S for $T \leq 1300°C$ but not for $T > 1300°C$. The oxidation resistance is better, however, with the UBE powder at all temperatures for the materials with $z = 3·8$.

The microstructure of the oxide scales formed on 0·5:3:U at $T > 1300°C$ is quite different from that of 0·5:3:S (see Fig. 10(e) later and 4(b)). The oxide scale is more fine-grained for 0·5:3:U, seems to contain less amorphous phase and also looks more porous; increasingly so with increasing temperature. To a certain extent the microstructure of the oxide scale thus reflects the microstructure of the bulk. According to the oxidation curves, the microstructure of the oxide scale formed on 0·5:3:U seems to lead to a less protective scale than that formed on 0·5:3:S at $T \geq 1300°C$. The oxide scales as well as the microstructure of the bulk materials 3·8:3:S and 3·8:3:U are very much alike, and the glassy phases in the oxide scales at 1400°C have approximately the same composition (3·8:3:U, 1:0·5:0·3 and 3·8:3:S, 1:0·4:0·4). For these ceramics it seems to be different amounts of impurity and not the differences in microstructure that have an influence on the oxidation resistance. The scale formed on the 3·8:0:U sialon seems, however, to contain a lower amount of mullite than that of 3·8:0:S.

3.1.3 Oxidation kinetics

Only a few of the obtained oxidation curves could be exhaustively described by the parabolic rate law. Four different types of oxidation curves could be recognized in this study. An example of each type is shown in Fig. 8. The first type obeys the parabolic law (3·8:3:U, $T = 1250°C$) throughout, i.e. the derivative of the $(\Delta w/A_0)^2$ versus t curve is constant. The second type of curve (3·8:3:S, $T = 1400°C$) has a shape such that the derivative of $(\Delta w/A_0)^2$ decreases with increasing time during the entire experiment. The third type of curve starts out the same as the second but after a certain time obeys the parabolic rate law (3·8:6:S, $T = 1400°C$). The last type of curve is somewhat different from the others (0·5:3:S, $T = 1350°C$) in that the derivative of $(\Delta w/A_0)^2$ increases at the outset, then suddenly decreases and finally become constant, i.e. assumes a parabolic rate law behaviour.

The curves of the second type could all be completely fitted by the arctan function given in eqn (4). A combination of an arctan function (for $t < t_0$, see above) and a parabolic function (for $t > t_0$, eqn

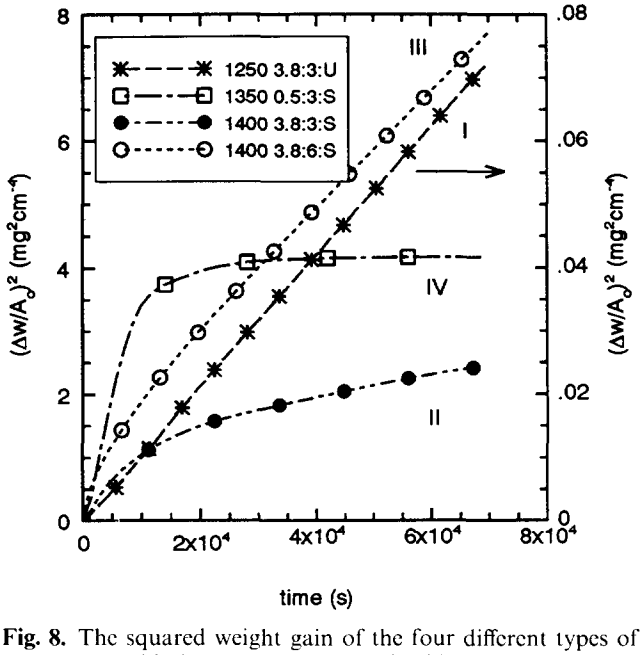

Fig. 8. The squared weight gain of the four different types of oxidation curves obtained in this study.

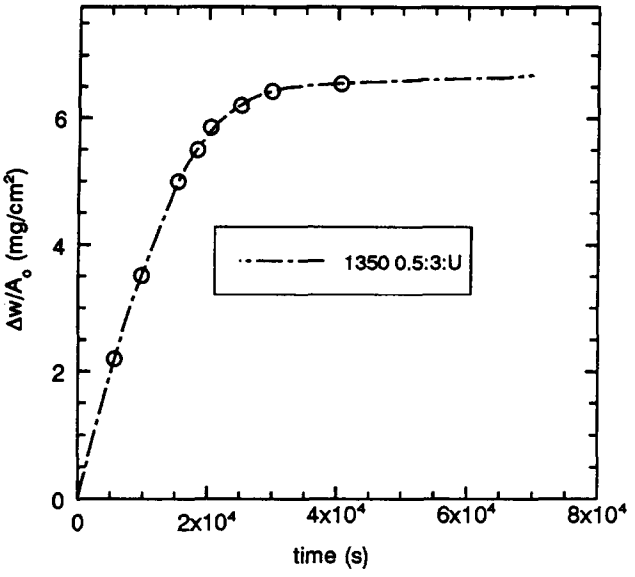

Fig. 9. The oxidation curve obtained for the sialon 0·5:3:U at 1350°C. The circles mark the duration of the eight short-time oxidation experiments performed.

(6)) could be used to describe the curves of the third type. All the curves yielded by oxidation of the materials 3·8:X:X and of 0·5:3/6:X for $T \leq 1300$°C could be fitted by a parabolic (type I), an arctan (type II) or a combination of an arctan and a parabolic function (type III). The fourth type of curve (type IV) comprises the ones that could not be described by an arctan function in any region; their final part could, however, be described by a parabolic function. This type of curve was observed for the material 0·5:3:S oxidized at 1300 and 1350°C for 0·5:3:U oxidized at 1300°C. Finally, the very small weight gains recorded for the material 0·5:0:S made it impossible to unambiguously determine the kinetics of the oxidation process.

3.1.4 Evolution of the oxide scale with time

Short-time oxidation experiments have been performed for the composition 0·5:3:U, yielding an oxidation curve of type IV, which could not be interpreted with the use of the arctan rate law. Pieces of this material were oxidized at 1350°C for 5000, 10 000, 15 000, 17 500, 20 000, 25 000, 30 000 and 40 000 s, as seen in Fig. 9. Micrographs of the oxide scales formed are shown in Fig. 10(a)–(d) and Fig. 11. The scale formed in the 5000 s oxidation is largely amorphous and contains large eruptions, presumably originating from the evolution of nitrogen, as seen in Fig. 10(a). The surface also contains islands of α-cristobalite grains surrounded by an amorphous phase with a higher concentration of Y than the main amorphous phase. The surface of the oxide

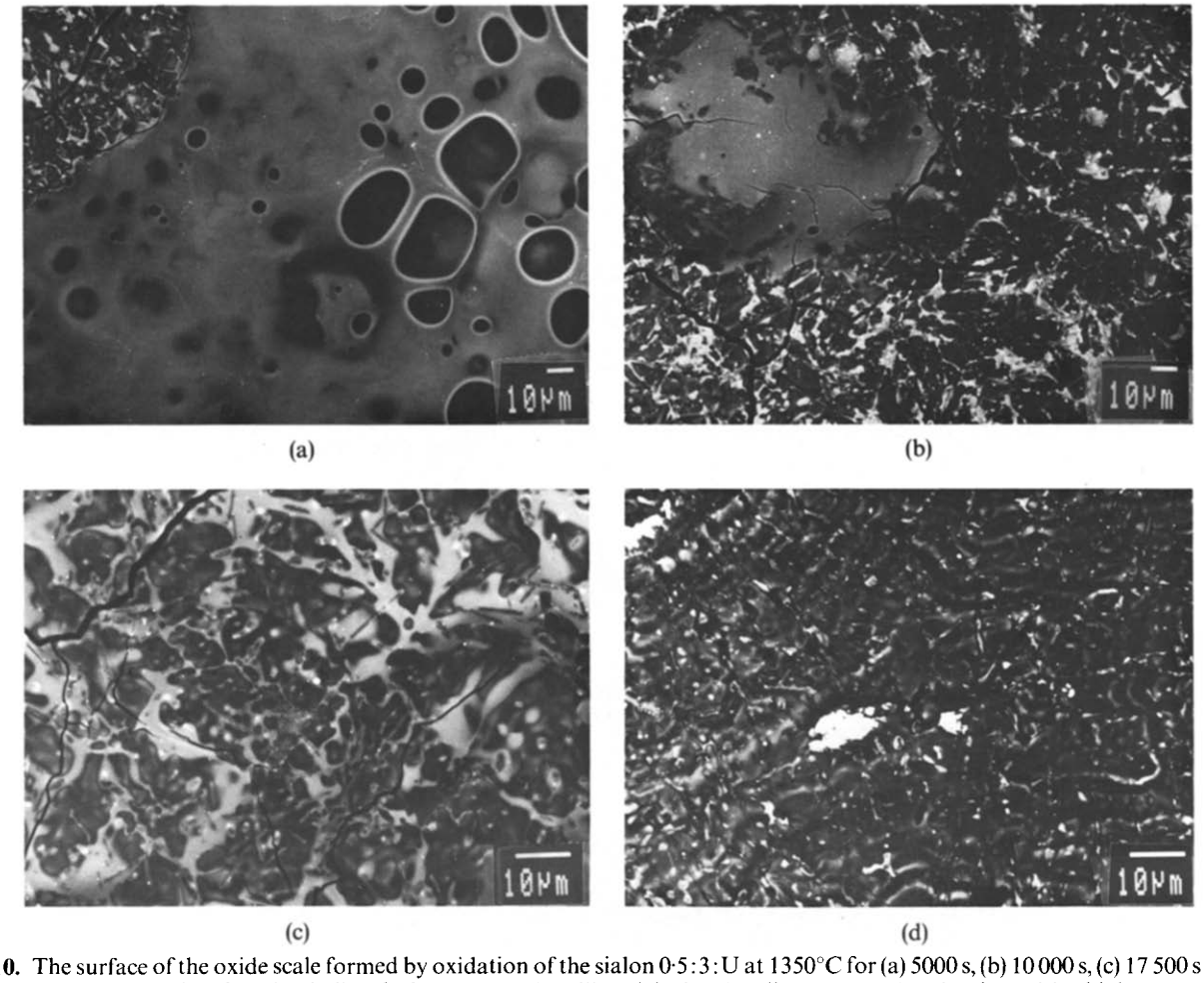

Fig. 10. The surface of the oxide scale formed by oxidation of the sialon 0·5:3:U at 1350°C for (a) 5000 s, (b) 10 000 s, (c) 17 500 s and (d) 25 000 s. The scales consist of α-cristobalite (darkest contrast), a silica-rich glass (medium contrast) and a glass with a high concentration of Y (lightest contrast).

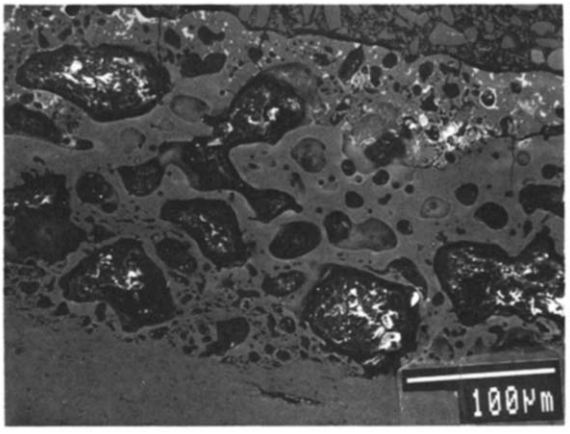

Fig. 11. Cross-section of the oxide scale formed during 10 000 s oxidation of 0·5:3:U.

scale formed by the 10 000 s oxidation is shown in Fig. 10(b). It consists mainly of α-cristobalite crystals surrounded by an amorphous phase. Larger amorphous areas are also observed. The cross-section of this oxide layer shows that most of the crystals are found at the surface, while the interior of the oxide scale is still amorphous (see Fig. 11). The surface and cross-section of the oxide scale are mainly composed of α-cristobalite grains after 17 500 s oxidation, and an yttrium-containing phase is found between the grains (Fig. 10(c)). The microstructure of the oxide scale formed after 25 000 s oxidation, just before the plateau of the oxidation curve in Fig. 9, is quite different from the one previously described, as seen in Fig. 10(d). The intergranular phase now only forms a very thin film between the silica grains or is gathered in multi-grain pockets. This microstructure is maintained during the final part of the oxidation experiment, where the parabolic rate law is obeyed. This study shows the kinetics of the oxidation to be closely related to the evolution of the oxide scale microstructure; the oxidation rate decreases due to crystallization. The initial, almost linear weight increase corresponds to formation of an amorphous oxide scale which is not entirely coherent (Fig. 10(a)). The ceramic will be exposed to the oxidizing atmosphere as the nitrogen bubbles break through the oxide scale, and the oxidation will not be solely diffusion controlled. As the oxide scale grows thicker and starts to crystallize, nitrogen bubbles will now only disrupt small parts of the scale when leaving the sample, implying that the oxidation rate will slow down and be controlled by diffusion. After the crystallization of the oxide scale the oxygen will reach the sialon matrix mainly through grain boundary diffusion. The evolution of the oxide scale during the oxidation corresponds to the general idea for the development of the new rate law. The fact that this rate law could not be used is most probably due to the relatively long duration of the initial linear oxidation period and the following very rapid crystallization process, i.e. the arctan regime is too short too be discerned.

3.1.5 Oxidation parameters

The rate constants and other parameters associated with the various rate equations are summarized in Table 3.

The parabolic rate constant, K_p, is found to increase with increasing temperature. The dependence of the rate constant on temperature is shown in an Arrhenius plot in Fig. 12(a) ($z = 3{\cdot}8$) and (b) ($z = 0{\cdot}5$). As seen in the figure, a linear relationship between $\ln(K_p)$ and $1/T$ is obtained for all materials with $z = 3{\cdot}8$, and the activation energy of the oxidation process can be determined. The oxidation rate and the activation energy of the process increases when yttria is added (3·8:0:S

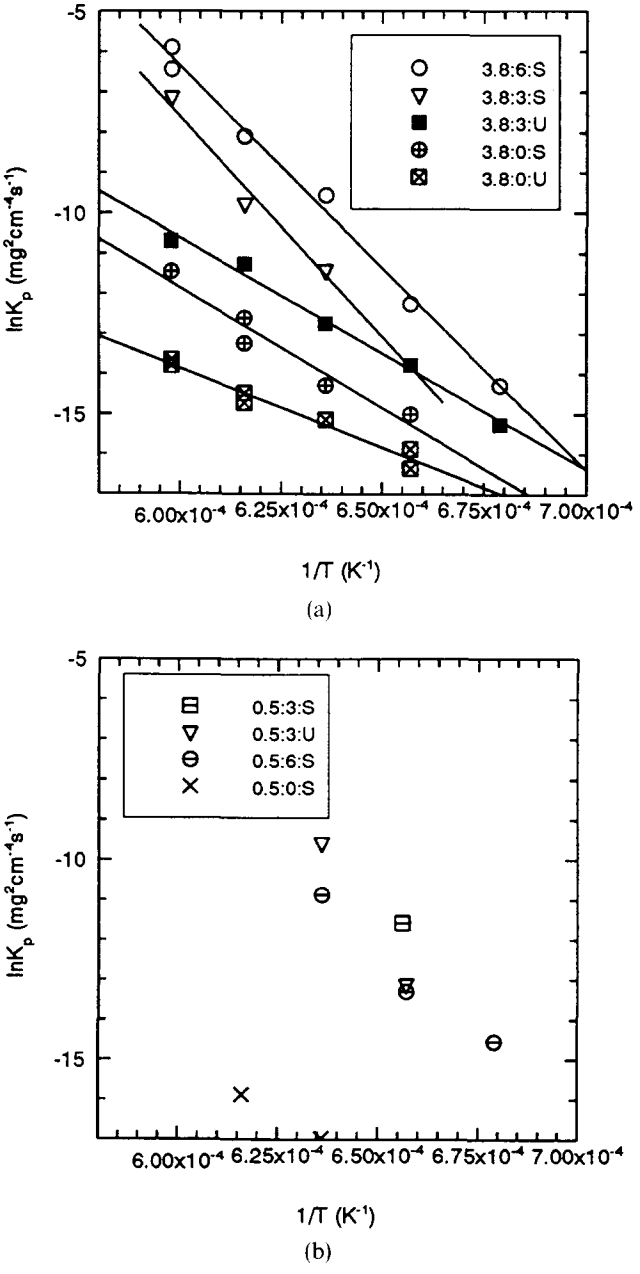

Fig. 12. Arrhenius plot of the parabolic rate constants calculated for the sialons with a z-value of (a) 3·8 and (b) 0·5.

Table 3. Oxidation parameters for the β-sialon materials

T (°C)	*Sample (z value:wt% yttria; Si_3N_4 powder (UBE or Starck)*								
	0·5:0:S	*0·5:3:S*	*0·5:3:U*	*0·5:6:S*	*3·8:0:S*	*3·8:0:U*	*3·8:3:S*	*3·8:3:U*	*3·8:6:S*
Oxidation kinetic[a]									
1 200	—	—	—	III	—	—	—	I	III
1 250	—	III	II	III	I	III	—	I	III
1 300	I[b]	IV	III	III	II	III	II	II	III
1 350	II	IV	IV	p	II	III	II	II	III
1 400	l	p	p	p	III	II	II	I	III
$\Delta w/A_0$ (mg cm^{-2}) after 20 h oxidation									
1 200	—	—	—	0·07	—	—	—	0·15	0·15
1 250	—	0·60	0·26	0·24	0·15	0·08	—	0·25	0·32
1 300	0·04[b]	0·60	0·39	0·38	0·10	0·11	0·42	0·28	0·33
1 350	0·03	2·0	5·6	1·45	0·25	0·17	0·56	0·45	0·70
1 400	0·05	6·8	11·3	7·5	0·31	0·24	1·5	1·30	2·80
1 450	2·10	—	—	—	1·8	—	—	—	—
$K_p \times 10^{-6}$ (mg^2 cm^{-4} s^{-1})									
1 200	—	—	—	0·478	—	—	—	0·23	0·62
1 250	—	9·36	1·98	1·68	0·302	0·126	—	1·04	4·72
1 300	0·04[b]	—	67·8	18·8	0·625	0·264	10·7	2·93	70·5
1 350	0·13	—	—	—	3·34	0·495	56·5	12·9	304
1 400					10·6	1·19	796	20·9	2 750
f									
1 200	—	—	—	0·22	—	—	—	1	0·62
1 250	—	0·64	0·10	0·58	1	0·71	—	1	0·42
1 300			0·07	0·19	0·23	0·74	0·24	0·45	0·08
1 350	0·03				0·19	0·82	0·16	0·28	0·06
1 400					0·25	0·43	0·07	1	0·16
t_0 (s)									
1 200	—	—	—	6 800	—	—	—		44 000
1 250	—	14 400	> 70 000	6 500		61 500	—		35 000
1 300		25 000[c]	20 700	17 200	> 70 000	49 100	> 70 000	> 70 000	38 000
1 350		20 000[c]	40 000[c]		> 70 000	32 000	> 70 000	> 70 000	46 000
1 400					25 000	> 70 000	> 70 000		40 000
$\beta \times 10^{-4}$ (s^{-1})									
1 200	—	—	—	4·11	—	—	—		0·88
1 250	—	1·0	0·232	6·44		0·40	—		2·30
1 300			12·7	4·38	2·16	0·79	16	1·5	19·0
1 350	1·88				1·60	1·59	8·94	3·6	18·0
1 400					3·03	0·35	5·09		51·6
$K_p^0 \times 10^{-7}$ (mg^2 cm^{-4} s^{-1})									
1 200	—	—	—	0·57	—	—	—		2·95
1 250	—	44·0		6·43		0·73	—		12·1
1 300		16·0	10·7	16·9		1·60			9·93
1 350		72·4	486			3·40			34·3
1 400					11·4				923
E_a (kJ/mol)				710 ± 140	500 ± 70	330 ± 30	939 ± 150	480 ± 30	830 ± 30

[a] I–IV, Different types of oxidation curves described in Section 3.1.3; p, oxidation curves exhibit a 'paralinear oxidation' behaviour; l, linear oxidation kinetics.
[b] During the first 6000 s.
[c] Start of the final parabolic part.

500 ± 70 kJ mol^{-1}; 3·8:3:S 900 ± 150 kJ mol^{-1}; 3·8:6:S 830 ± 30 kJ mol^{-1} and 3·8:0:U 330 ± 30 kJ mol^{-1}; 3·8:3:U 480 ± 30 kJ mol^{-1}). The lowest rate constant and also the lowest activation energy are obtained for the material 3·8:0:U. A comparison of the K_p and E_a values obtained for the samples 3·8:0:S and U and 3·8:3:S and U shows that the samples prepared from Starck powder exhibit much higher rate constants and activation energies than those of the UBE materials. In this connection it can be noted that the Starck powder contains more impurities than the UBE powder. These results show that the oxidation rate and the activation energy of the process increase with increasing amount of intergranular phase and suggest that the presence of even small amounts of impurities will lead to an increased oxidation rate and activation energy. The presence of impurities in the glassy phases is believed to decrease the viscosity of the glass, resulting in a higher ion mobility.[1,10]

Equations (1), (4) and (6) have been used to determine the rate constants for $z = 3·8$, while for

$z = 0{\cdot}5$ the corresponding equations could only be satisfactorily applied when relatively low weight gains were observed, that is, when the initial linear oxidation was brief and the crystallization is relatively slow. These limitations have not been observed in the oxidation of sialons with $z = 3{\cdot}8$, where the nitrogen concentration is lower. The determined rate constants for the sialons with $z = 0{\cdot}5$ are given in Fig. 12(b). The oxidation rate of 0·5:0:S is very low (lower than for 3·8:0:U and S) and the addition of yttria decreases the oxidation resistance considerably, as also observed for $z = 3{\cdot}8$ (see above). As only a few rate constants could be evaluated for the material with $z = 0{\cdot}5$, the activation energies for the oxidation processes could not be determined. All the rate constants obtained are, however, of approximately the same magnitude as those determined for the corresponding materials with $z = 3{\cdot}8$. The rate constants determined for 0·5:3:S and U at 1250°C verify the conclusion already drawn, that higher rate constants are observed for materials containing the larger amount of impurities. At $T > 1300$°C, however, where a parabolic rate constant could not be determined, it was found that $(\Delta w/A_0)$ after 70 000 s oxidation was higher for 0·5:3:S than for 0·5:3:U. As the complementary short-time oxidation experiments already described show, this could be explained by the oxidation kinetics being dependent on the microstructure of the oxide scale. The amount of impurities has in this case only a minor influence on the oxidation behaviour. The material 0·5:6:S seems to have an equal or even a somewhat lower oxidation rate than the materials containing less yttria. This contradicts the observation for $z = 3{\cdot}8$ but might be explained by the observation that 0·5:6:S, apart from β-sialon, also contains minor amounts of α-sialon, which is known to incorporate yttrium in its structure. This in its turn results in a material containing a lower amount of intergranular glassy phase (see Table 2).

The f values, defined in eqns (3) and (5) and interpreted to represent the degree of divergence from the pure parabolic rate-law behaviour, are found in Table 3. The discrepancy could be due to either: (i) a continuous decrease due to crystallization of the cross-section area available for the rapid diffusion in the oxide scale; (ii) a decrease of the available diffusion pathways in the matrix by the formation of a depleted zone and/or by crystallization of the intergranular phase, whereby diffusion of ions from the intergranular phase into the oxide scale is hindered; or (iii) a combination of (i) and (ii).

f is found to be higher for the materials with $z = 3{\cdot}8$ prepared from the Si_3N_4 powder containing the lower amount of impurities, as seen in Table 3. Previous reports have shown that impurities promote crystallization,[1,10,29] which the f values observed here for $z = 3{\cdot}8$ also indicate. This corresponds to the higher amount of mullite crystals found by the SEM studies in the oxide scale on 3·8:0:S compared to 3·8:0:U. The oxide scale formed on 0·5:3:U was, however, observed to be more crystalline than the scale formed on 0·5:3:S. This is also reflected by a lower f value observed at 1250°C. For these ceramics the microstructure of the oxide scale seemed, in addition to the amount of impurities, to be dependent on the microstructure of the bulk material. In general, f is found to decrease with increasing amount of yttria and with increasing temperature. For the remainder of the materials it is, however, impossible to link the calculated f values to an observed degree of crystallinity of the oxide scales or to the thickness of the depleted zone judged by X-ray analysis and by inspection of the oxide scales in the SEM. The unexpectedly high f value obtained for the ceramic 3·8:3:U at 1400°C cannot at the moment be accounted for. No differences have been observed between the microstructure of this oxidized material and the materials 3·8:3:S and 3·8:6:S. One difference compared to temperatures below 1400°C for $z = 3{\cdot}8$ is, however, that at 1400°C, which is higher than the eutectic temperature of the Si–Al–Y–O system, no Y-containing crystals but only a glass forms in the oxide scale. However, it ought to be noted that the f values are only approximate, due to the difficulties associated with the determination of t_0, which is needed for the calculation of f (eqns (5) and (7), see also Ref. 30).

The apparent rate constants, K_p^0, obtained from the final parabolic part of the oxidation curves, are shown in an Arrhenius plot in Fig. 13. As expected,

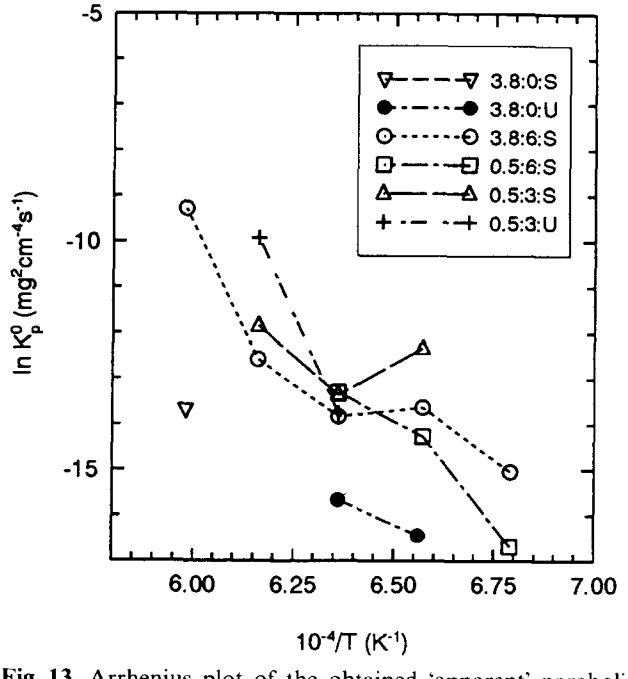

Fig. 13. Arrhenius plot of the obtained 'apparent' parabolic rate constants, K_p^0 (eqn (6)).

these constants do not show a linear relationship with T^{-1}, as this rate constant according to eqn (7) depends both on the K_p and the f value.

Table 3 gives values of β, the rate of decrease of $A(t)$, for the different oxidation experiments. β is observed to increase with increasing amount of yttria in the material and with increasing amount of impurities, but no obvious dependence of β on temperature is found.

Repeated oxidation experiments using the same material have shown that the final weight gains are in agreement with each other within $\pm 20\%$. The differences in final weight gain between the oxidation experiments have been shown to be dependent on the evolution of the microstructure of the oxide scale with time (or alternatively the evolution of the intergranular phase). However, by interpretation of the weight gain curves using the actan rate law, it is possible to obtain both consistent parabolic rate constants and a value of the divergence from a pure parabolic behaviour (f value). These parameters can more satisfactorily be used in comparing the oxidation behaviour of different materials than the final weight gains and/or K_p^0 values. For example, the final weight gain is higher for 3·8:6:S than for 3·8:3:S at 1300°C, but the opposite is found for the calculated K_p values. This is due to the fact that the final weight gain depends on both the oxidation rate constant, K_p, the f value and the rate constant, β. The calculated rate constants are reproduced within $\pm 15\%$, while corresponding values for the final weight gain agree within $\pm 20\%$.

3.2 A comparison of the oxidation behaviour of Si_3N_4 and β-sialons with $z = 1$, 2·5 and 3.8 prepared from UBE powder

3.2.1 Characterization of the prepared samples

Single-phase β-sialon ceramics were obtained according to X-ray diffraction. The cell parameters of the β-phase, the calculated z values and the densities are given in Table 4. TEM studies of single-phase β-sialons prepared with the same method as in this paper have previously been reported to yield β-sialon ceramics almost free from an intergranular phase. It was also reported that the grain size increased with increased z.[28,31]

3.2.2 Oxidation curves and characterization of oxide scales

The squared weight gains recorded versus time during the oxidation of Si_3N_4 and sialons with $z = 1$, $z = 2{\cdot}5$ and $z = 3{\cdot}8$ are shown in Fig. 14(a)–(d), respectively. The figures show that almost all of the oxidation curves deviate from a parabolic rate law. The divergence from the parabolic rate law is larger for Si_3N_4 and for the β-sialon with $z = 1$ than for the sialons with $z = 2{\cdot}5$ and 3·8, and then the final weight gain increases more clearly with increasing temperature for the higher z values.

The microstructures of the oxide scale surfaces differ considerably between the different materials. Crystals of α-cristobalite and tridymite are observed on Si_3N_4 (the relative amount of the two phases alters with temperature). SEM studies of the surface of the oxide scale, formed on the sialon of the composition $z = 1$, reveals it to be mainly amorphous, but a minor amount of small crystals of mullite composition is also found. The X-ray diffraction patterns of the oxide scales show, however, that the scales contain α-cristobalite.

The surface is very even, and voids originating from the evolution of nitrogen have not been observed. The surface of the oxide scale formed on the sialons with $z = 2{\cdot}5$ is rough, consisting of glass bubbles, mullite crystals and a few voids originating from the nitrogen evolution. X-Ray diffraction from the oxide scale reveals that it also contains minor amounts of α-cristobalite. The scale formed on the sialon with a z value of 3·8 has a microstructure similar to the one just described but contains less glass and more mullite crystals.

The glassy phase formed in the oxide scale will be an Si–Al–O glass. A silica glass can, however, not incorporate more than 5–10 mol% Al_2O_3 in its structure. The substitution of Al^{3+} for Si^{4+} in tetrahedral coordination will lead to a glass with a denser structure, as the oxygen must bridge three tetrahedra rather than two to maintain charge balance. If more Al_2O_3 is present, two glasses of different compositions will form. The second glass will have an approximate mullite composition, containing Al in octahedral coordination as well.[32] If a completely amorphous oxide scale is formed on

Table 4. Properties of the single-phase β-sialon materials prepared from UBE powder

Designated z-value	*a-axis (nm)*	*c-axis (nm)*	*Calculated z-value*	*Density (g cm^{-3})*	*Theoretical density (g cm^{-3})*
0[a]	0·760 1	0·290 7	—	3·146	3·203
1	0·763 0	0·293 0	0·90	3·120	3·163
2·5	0·767 3	0·296 8	2·38	3·039	3·102
3·8	0·770 0	0·300 0	3·56	3·052	3·060

[a] From Ref. 8.

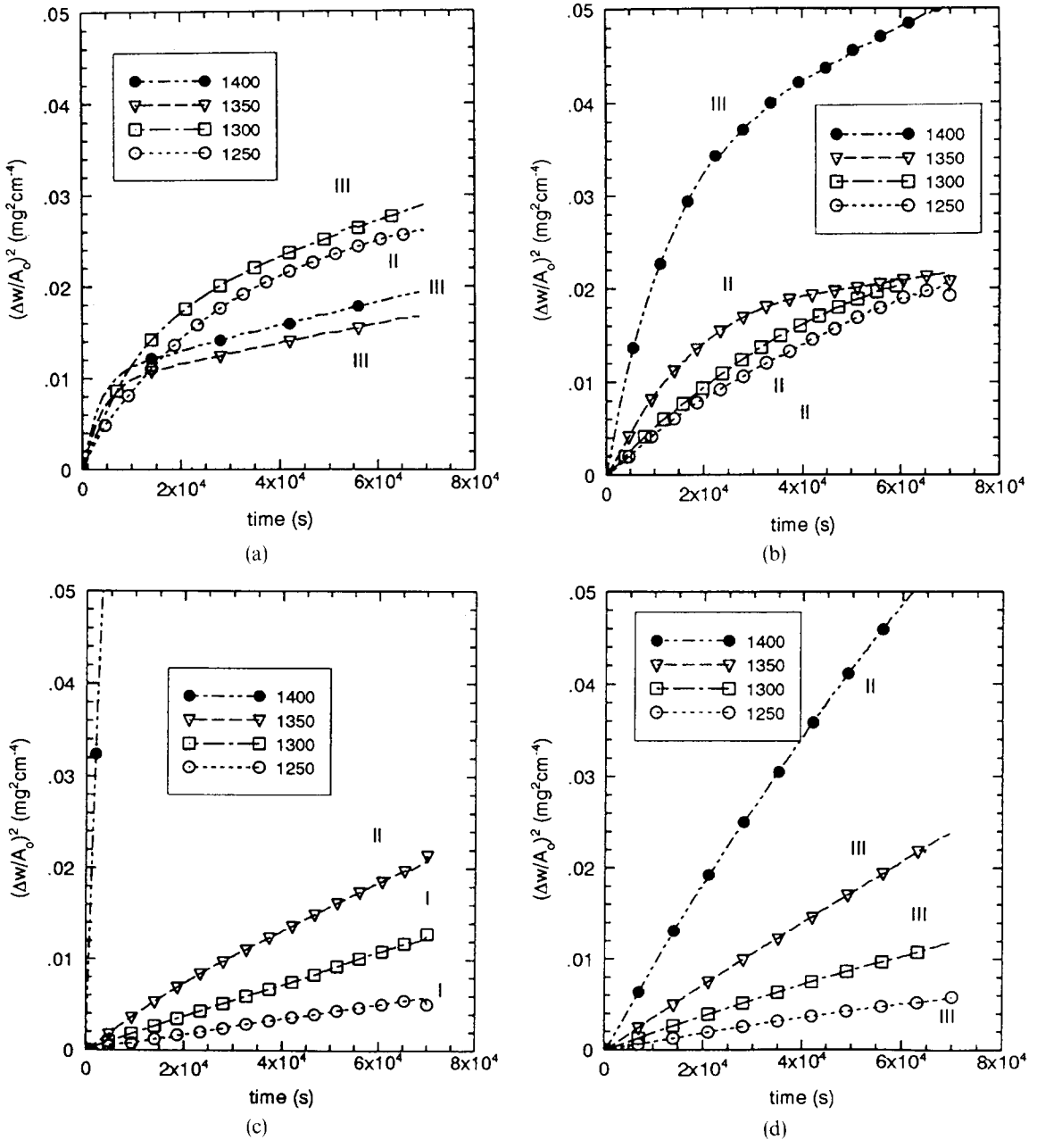

Fig. 14. The squared weight gain recorded during oxidation of (a) Si_3N_4, (b) $z = 1$, (c) $z = 2{\cdot}5$ and (d) $z = 3{\cdot}8$. The roman numerals denote the determined oxidation kinetics, as defined in Section 3.1.3.

the β-sialon, the scale on the sialon with $z = 1$ will consist of a glass with 9 mol% Al_2O_3, while on the sialons with $z = 2{\cdot}5$ and $3{\cdot}8$ two glasses will form, one with approximately the same composition as on that with $z = 1$ and one with mullite composition. Mullite crystals as well as α-cristobalite are, however, present in all of the oxide scales, in addition to a glassy phase. A phase separation of the glass has not been observed. On the contrary, the EDS analysis showed that the glassy phases on the sialons with $z = 1$, $2{\cdot}5$ and $3{\cdot}8$ have approximately the same composition (8–12 mol% Al_2O_3). This observation may suggest that the glass with the mullite composition has crystallized.

3.2.3 Oxidation kinetics

Only a few of the obtained weight gain curves could be described by the ordinary parabolic rate law (referred to previously as type I curve). The other oxidation curves could be classified either as type II or III. No curve of type IV was obtained. The curves of the type I can, however, also be interpreted as type III, but the deviation from a pure parabolic rate law is very small, which makes it very difficult to obtain a satisfactory fit of the arctan function to the experimental curve. These curves have therefore been interpreted with use of the parabolic rate law.

3.2.4 Oxidation parameters

The parabolic rate constants, f values and the other parameters associated with the oxidation curves are found in Table 5.

As Si_3N_4 and the β-sialons are expected to be almost free from intergranular glass, the oxidation

Table 5. Oxidation parameters for Si_3N_4 and single-phase β-sialons

T (°C)	*Sample (z-value)*[a]			
	Si_3N_4[b]	*1*	*2·5*	*3·8*
Oxidation kinetic[c]				
1 250	II	II	I	III
1 300	III	II	I	III
1 350	III	III	III	III
1 400	III	III		II
$\Delta w/A_0$ (mg cm^{-2}) after 20 h oxidation				
1 250	0·16	0·13	0·04	0·08
1 300	0·17	0·13	0·08	0·11
1 350	0·13	0·13	0·12	0·17
1 400	0·14	0·22	1·0	0·24
$K_p \times 10^{-6}$ (mg^2 cm^{-4} s^{-1})				
1 250	1·12	0·63	0·08	0·126
1 300	2·12	0·68	0·18	0·264
1 350	5·88	1·31	0·48	0·495
1 400	12·2	3·70		1·190
f				
1 250	0·18	0·46	1	0·71
1 300	0·12	0·46	1	0·74
1 350	0·05	0·10	0·65	0·82
1 400	0·04	0·14		0·43
t_0 (s)				
1 250	> 70 000	> 70 000		61 500
1 300	41 000	> 70 000		49 100
1 350	18 500	41 000	35 200	32 000
1 400	17 000	41 400		> 70 000
$\beta \times 10^{-4}$ (s^{-1})				
1 250	0·47	0·52		0·40
1 300	1·12	0·45		0·79
1 350	4·79	0·42	0·4	1·52
1 400	8·61	0·95		0·35
$K_p^0 \times 10^{-7}$ (mg^2 cm^{-4} s^{-1})				
1 250				0·73
1 300	1·74			1·60
1 350	1·40	0·823	2·61	3·41
1 400	1·28	2·81		
E_a (kJ/mol)	310 ± 25	320 ± 40	360 ± 40	330 ± 30

[a] These ceramics are prepared from UBE powder.
[b] Data from Ref. 8.
[c] I–IV, Different types of oxidation curves described in Section 3.1.3.

rate ought to be dependent on the oxygen diffusion rate through the oxide scale. The f value, which denotes the degree of divergence from the parabolic rate law, is in this case interpreted to be due to a partial crystallization of the oxide scale. The f values are found to decrease with increasing temperature, as also observed previously for the sialon materials containing Y_2O_3. The f value is also found to increase with increased amount of alumina. The SEM studies of the surfaces and of the cross-sections of the oxide scales did not, however, reveal an increasing amount of amorphous phase with increasing Al^{3+} content. Instead, the opposite trend seemed to be valid. The X-ray diffraction studies show that α-cristobalite is present in the oxide scales, but in diminishing amounts with increasing z-value. This observation indicates that the formation of α-cristobalite rather than mullite is the reason for the more pronounced divergence from the parabolic rate law for ceramics with small z values. The mullite crystals are small and needle-like, while the silica crystals are larger and globular. The needle shape of the mullite crystals will probably result in more oxygen diffusion pathways being present in the scales containing mainly mullite crystals, compared to those containing mainly α-cristobalite grains. Thus, the difference in the obtained f values is most probably explained by the differences in grain shape between the crystalline phases.

The parabolic rate constants were found to increase with increasing temperature for the Si_3N_4 and the sialon ceramic with $z = 1$, even though the final weight gain did not increase with increasing temperature. The rate constants were found to decrease with increasing z value, but the ones determined for the sialons with $z = 2{\cdot}5$ and $3{\cdot}8$ are almost equal, or even somewhat lower for $z = 2{\cdot}5$. The $\ln(K_p)$ values decrease linearly with $1/T$ for all ceramics as seen in Fig. 15, but the activation energy does not vary significantly with increasing z value, which indicates that the oxidation mechanism is the same for all the materials studied.

The parabolic rate constants were determined by measuring the weight gain associated with the substitution of oxygen for nitrogen during the oxidation. However, as the nitrogen concentration decrease with increased z value, the thickness of the formed oxide scale must increase with increasing z value for a given weight gain. If the oxygen diffusion rates through the oxide scale are to be compared for

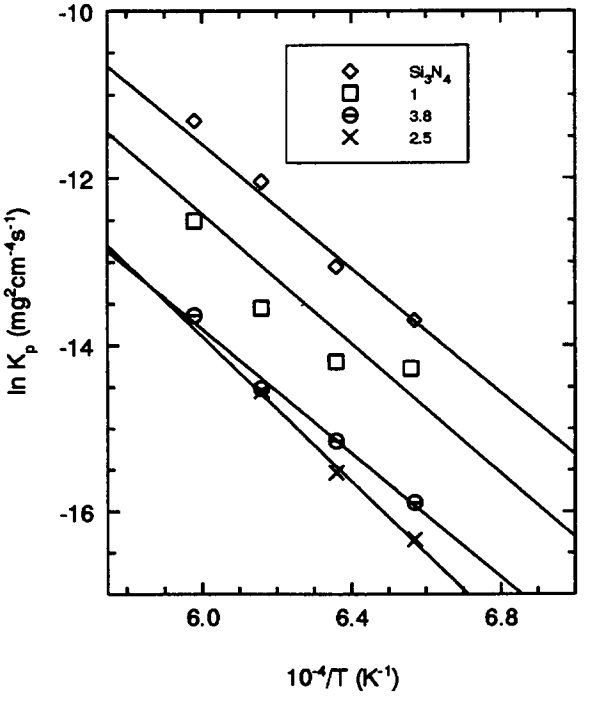

Fig. 15. Arrhenius plot of the parabolic rate constants, K_p, for Si_3N_4 and the β-sialons with $z = 1$, 2·5 and 3·8.

the different sialon ceramics, the weight gain has to be converted to thickness of the oxide layer. The relation between the weight gain, $\Delta w/A_0$, and the thickness of the oxide scale, X, is

$$\Delta w/A_0 = \rho_e X \tag{8}$$

where ρ_e is an 'effective density' of the oxide scale, calculated as

$$\rho_e = (M_{O_2} n_{O_2} - M_{N_2} n_{N_2})/(\sum n_i M_i/\rho_i) \tag{9}$$

where M_{O_2}, M_{N_2} and M_i are the molar masses of oxygen, nitrogen and the formed oxides, ρ_i is the density of the oxides in the oxide scale and n_{N_2}, n_{O_2} and n_i are the amounts of nitrogen released, oxygen absorbed and the amounts of oxides formed according to the reaction

$$Si_{6-z}Al_zO_zN_{8-z} + (24-3z)/4O_2 \rightarrow (18-4z)/3\ SiO_2 + z/6\ Al_6Si_2O_{13} + (8-z)/2\ N_2 \tag{10}$$

The density of the oxide scale can only be roughly estimated, because the relative amounts of the crystalline phases and an amorphous phase cannot be determined. The density is estimated to a value between the density of silica glass, 2·2 g cm^{-3}, and that of a completely crystalline scale consisting of mullite and silica, 2·32 g cm^{-3} for Si_3N_4, to 2·9 g cm^{-3} for $z = 3{\cdot}8$. By replacing $(\Delta w/A_0)$ with X, the parabolic rate law will read

$$X = (K_p/\rho_e^2)\sqrt{t} + C, \text{ or } X = \alpha\sqrt{t} + C \tag{11}$$

where α denotes the growth rate of the oxide scale. The α values for Si_3N_4 and the sialons are shown in an Arrhenius plot in Fig. 16, and they are found to decrease for the various ceramics in the order Si_3N_4, $z = 1$, $z = 3{\cdot}8$ and $z = 2{\cdot}5$, but the α values for the sialons are very close. This is as expected, because the glassy phases in the oxide scale have approximately the same composition. It has previously been proposed that the decreased oxidation rate for sialons with an increasing z value is due to the different concentrations of nitrogen or to the formation of mullite crystals.[1,2,10] In addition, the present study indicates that a small amount (< 10 mol%) of alumina in the silica glass of the oxide layer yields a denser glass structure, which seems to decrease the diffusion rate of oxygen through the oxide scale. Furthermore, the observed low weight gain and the low f value for Si_3N_4 and for the sialon with $z = 1$ can be explained by the formation of α-cristobalite crystals. That is, the formation of α-cristobalite in the oxide scale results in a more protective scale than a corresponding formation of mullite.

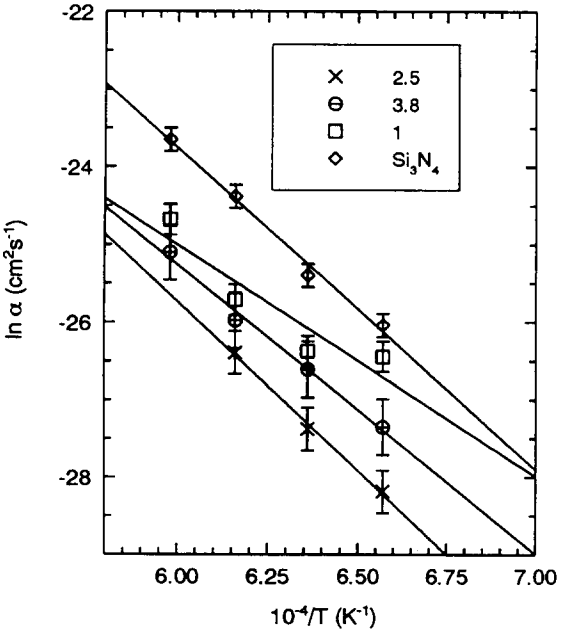

Fig. 16. Arrhenius plot of the growth rate of the oxide scale, α, (eqn (9)) for Si_3N_4 and β-sialons with $z = 1$, 2·5 and 3·8. The end-points of the bars correspond to ρ_e (eqn (8)) of a completely amorphous ($\rho_{oxid} = 2{\cdot}2$ g cm^{-3} for all compositions), and a complete crystalline oxide scale, respectively, according to eqn (9).

4 Conclusions

(1) The oxidation resistance of the sialons with $z = 0{\cdot}5$, containing a Y-containing intergranular glass, is better at $T \leq 1300$°C but worse at $T \geq 1300$°C than that of the sialons with $z = 3{\cdot}8$.

(2) The rate law

$$(\Delta W/A_0) = a \arctan\sqrt{bt} + c\sqrt{t} + d,$$

alone or in combination with the parabolic rate law, could be satisfactorily used for interpretation of the oxidation kinetics of all of the β-sialons, except for $z = 0{\cdot}5$ with 3 and 6 wt% yttria at $T \geq 1300$°C.

(3) Parabolic rate constants and activation energies could be determined by fitting the arctan function to the experimental curves. The rate constant and the activation energy were found to increase with increasing amount of intergranular phase; and the K_p and α values were found to be lower for the single-phase β-sialons than for Si_3N_4, but the activation energy was approximately the same.

(4) When the arctan function could not be applied to interpret the oxidation kinetics, the oxidation process seemed anyhow to be closely related to the evolution of the oxide scale with time. In this case, the oxidation was found to be very rapid at the beginning of the process but considerably slower later on. The decrease seems to be related to a rapid crystallization of the oxide scale.

(5) The oxidation resistance was found to be much higher for the materials with $z = 3{\cdot}8$ (0 and 3 wt% yttria), prepared from the Si_3N_4 powder with a lower amount of impurities, than for materials obtained from the powder with a higher amount of impurities. Both the rate constant, K_p, and the activation energy were lower for the materials with a smaller amount of impurities. The same conclusion could also be drawn from oxidation of the material with $z = 0{\cdot}5$ (3 wt% yttria) at $T \leq 1300°C$ but not for $T > 1300°C$. The factor dominating the oxidation rate at $T > 1300°C$ seemed instead to be the evolution of the microstructure of the oxide scales.

(6) The parabolic rate constants are lower for the single-phase β-sialons than for Si_3N_4. This might be due to the fact that the glass containing aluminium is denser than a pure silica glass.

(7) For Si_3N_4 and the single-phase β-sialons the divergence from parabolic oxidation is most pronounced for low z values, where a high amount of α-cristobalite is present in the oxide scales.

Acknowledgement

The authors gratefully acknowledge the interest of Dr Per-Olov Käll in this work and his contribution to the development of the new rate law. This work has been financially supported by the Swedish Board for Industrial and Technical Development.

References

1. Singhal, S. C., Oxidation of silicon nitride and related materials. In *Nitrogen Ceramics*, ed. F. L. Riley. Noordhoff, Leiden, The Netherlands, 1977, pp. 607–26.
2. Schlichting, J., Oxidation and hot corrosion behavior of Si_3N_4 and sialon. In *Nitrogen Ceramics*, ed. F. L. Riley. Noordhoff, Leiden, The Netherlands, 1977, pp. 627–34.
3. Du, H., Tressler, R. E., Spear, K. E. & Pantano, C. G., Oxidation studies of crystalline CVD silicon nitride. *J. Electrochem. Soc.*, **136** (1989) 1527–35.
4. Du, H., Houser, C. A., Tressler, R. E., Spear, K. E. & Pantano, C. G., Isotopic studies of oxidation of Si_3N_4 and Si using SIMS. *J. Electrochem. Soc.*, **137** (1990) 741–2.
5. Choi, D. J., Frischbach, D. B. & Scott, W. D., Oxidation of chemically-vapor-deposited silicon nitride and single crystal silicon. *J. Am. Ceram. Soc.*, **72** (1989) 1118–23.
6. Ogbuji, L. U. J. T., Role of Si_2N_2O in passive oxidation of chemically-vapor-deposited Si_3N_4. *J. Am. Ceram. Soc.*, **75** (1992) 2995–3000.
7. Singhal, S. C., Thermodynamic analysis of the high-temperature stability of silicon nitride and silicon carbide. *Ceram. Int.*, **2** (1976) 123–30.
8. Persson, J., Käll, P.-O. & Nygren, M., Parabolic–non-parabolic oxidation kinetic of Si_3N_4. *J. Eur. Ceram. Soc.*, **12** (1992) 177–84.
9. Ekström, T. & Nygren, M., SiAlON ceramics. *J. Am. Ceram. Soc.*, **75** (1992) 1259–76.
10. Sorrell, C. C., Silicon nitride and related nitrogen ceramics: II. Phase equilibria and properties of reaction bonded and hot pressed Si–Al–O–N systems. *J. Am. Ceram. Soc.*, **19** (1983) 48–67.
11. Clarke, D. R., Thermodynamic mechanism for cation diffusion through an intergranular phase. In *Progress in Nitrogen Ceramics*, ed. F. L. Riley. Martius Nijhoff, The Hague, 1983, pp. 421–6.
12. Clarke, D. R. & Lange, F. F., Oxidation of Si_3N_4 alloys: relationship to phase equilibria in the system Si_3N_4–SiO_2–MgO. *J. Am. Ceram. Soc.*, **63** (1980) 586–93.
13. Billy, M. & Desmaison, J. G., High temperature oxidation of silicon-based structural ceramics. *High Temperature Technology*, **4** (1986) 131–9.
14. Babini, G. N., Bellosi, A. & Vincenzini, P., A diffusion model for the oxidation of hot-pressed Si_3N_4–Y_2O_3–SiO_2 materials. *J. Mat. Sci.*, **19** (1984) 1029–42.
15. Cubicciotti, D. & Lau, K. H., Kinetics of oxidation of hot-pressed silicon nitride containing magnesia. *J. Am. Ceram. Soc.*, **61** (1978) 512–17.
16. Lewis, M. H. & Barnard, P., Oxidation mechanism in Si–Al–O–N ceramics. *J. Mat. Sci.*, **15** (1980) 443–8.
17. Cubicciotti, D. & Lau, K. H., Oxidation of yttria hot-pressed silicon nitride. *J. Electrochem. Soc.*, **126** (1979) 1723–6.
18. Echeberria, J. & Castro, F., Comparison between continuous and cyclic oxidation of fully dense Si_3N_4. In *Structural Ceramics—Processing, Microstructure and Properties*, ed. J. J. Bentzen *et al.* Roskilde, Denmark, 1990, pp. 249–55.
19. Andrews, P. & Riley, F. L., The microstructure and composition of oxide films formed during high temperature oxidation of sintered silicon nitride. *J. Eur. Ceram. Soc.*, **5** (1989) 245–56.
20. Andrews, P. & Riley, F. L., Silicon nitride oxidation/re-oxidation. *J. Eur. Ceram. Soc.*, **7** (1991) 125–32.
21. Nickel, K. G., Danzer, R., Schneider, G. & Petzow, G., Corrosion and oxidation of advanced ceramics. *Pow. Met. Int.*, **21** (1989) 29–33.
22. Pomeroy, M. & Hampshire, S., Oxidation processes in silicon-nitride based ceramics. *Mat. Sci. Eng.*, **A109** (1989) 389.
23. Chen, J., Sjöberg, J., Lindquist, O., O'Meara, C. & Pejryd, L., The rate-controlling processes in the oxidation of HIPed Si_3N_4 with and without sintering additives. *J. Eur. Ceram. Soc.*, **7** (1991) 319–27.
24. Tripp, W. C. & Graham, H. C., Oxidation of Si_3N_4 in the range 1300 to 1500°C. *J. Am. Ceram. Soc.*, **59** (1976) 399–403.
25. Pomeroy, M. J. & Hampshire, S., Oxidation process in a high substitution β'-sialon. *Mat. Chem. Phys.*, **13** (1985) 437–48.
26. Wang, L., He, C. & Wu, J. G., Oxidation of sintered silicon nitride: I. Phase composition and microstructure. *Mat. Sci. Eng.*, **A157** (1992) 125–30.
27. Wang, L., He, C. & Wu, J. G., Oxidation of sintered silicon nitride materials. In *Ceramic Materials and Components for Engines*, ed. V. J. Tennery. Las Vegas, 1988, pp. 604–11.
28. Ekström, T., Käll, P.-O., Nygren, M. & Olsson, P.-O., Dense single-phase β-sialon ceramics by glass-encapsulated hot isostatic pressing. *J. Mat. Sci.*, **24** (1989) 1853–61.
29. Persson, J., Käll, P.-O. & Nygren, M., Oxidation kinetics of Si_2N_2O ceramics. In *Mat. Res. Soc. Symp. Proc.*, Vol. 287, ed. I-W. Chen *et al.* Boston, 1992, pp. 521–6.
30. Persson, J., Käll, P.-O. & Nygren, M., Interpretation of the parabolic and nonparabolic oxidation behaviour of silicon oxynitride. *J. Am. Ceram. Soc.*, **75** (1992) 3377–84.
31. Ekström, T. & Olsson, P.-O., β-Sialon ceramics prepared at 1700°C by hot isostatic pressing. *J. Am. Ceram. Soc.*, **72** (1989) 1722–4.
32. MacDowell, J. F. & Beall, G. H., Immiscibility and crystallization in Al_2O_3–SiO_2 glasses. *J. Am. Ceram. Soc.*, **52** (1969) 17–25.